Dilepton production in nucleus-nucleus collisions at top CERN Super Proton Synchrotron energy of 158*A* GeV within the parton-hadron-string dynamics transport approach

O. Linnyk*
Institut für Theoretische Physik, Universität Giessen, DE-35392 Giessen, Germany

E. L. Bratkovskaya
Institut für Theoretische Physik, Johann Wolfgang Goethe University, 60438 Frankfurt am Main, Germany, and Frankfurt Institute for Advanced Studies, DE-60438 Frankfurt am Main, Germany

V. Ozvenchuk
Frankfurt Institute for Advanced Studies, DE-60438 Frankfurt am Main, Germany

W. Cassing
Institut für Theoretische Physik, Universität Giessen, DE-35392 Giessen, Germany

C. M. Ko
Cyclotron Institute and Department of Physics and Astronomy, Texas A&M University, College Station, Texas 77843-3366, USA
(Received 18 July 2011; revised manuscript received 11 October 2011; published 28 November 2011)

Dilepton production in In + In collisions at 158*A* GeV is studied within the microscopic parton-hadron-string dynamics (PHSD) transport approach that incorporates explicit partonic degrees of freedom and dynamical hadronization as well as the more familiar hadronic dynamics in the final reaction stages. A comparison to the data of the NA60 Collaboration shows that the measured dilepton yield is well described by including the collisional broadening of vector mesons, while simultaneously accounting for the electromagnetic radiation of the strongly coupled quark-gluon plasma (sQGP) via off-shell quark-antiquark annihilation, quark annihilation with additional gluon bremsstrahlung, and the gluon-Compton scattering mechanisms. In particular, the spectra in the intermediate mass range (1 GeV $\leqslant M \leqslant$ 2.5 GeV) are dominated by quark-antiquark annihilation in the nonperturbative QGP. Also, the observed softening of the transverse mass spectra at intermediate masses (1 GeV $\leqslant M \leqslant$ 2.5 GeV) is approximately reproduced. Furthermore, for dileptons of low masses ($M <$ 0.6 GeV), we find a sizable contribution from the quark annihilation with additional gluon bremsstrahlung, thus providing another possible window for probing the properties of the sQGP.

DOI: 10.1103/PhysRevC.84.054917 PACS number(s): 25.75.Cj, 25.75.Nq, 24.85.+p

I. INTRODUCTION

Electromagnetic probes, i.e., dileptons and photons, are powerful tools to explore the early hot, dense stage of heavy-ion collisions as they are essentially unaffected by final-state interactions. Through their invariant mass and momentum distributions, they carry to the detector information about the conditions and properties of the environment in which they are emitted, thus providing a glimpse deep into the bulk of the strongly interacting matter created in these collisions [1,2]. In particular, dileptons have been suggested as probes of the quark-gluon plasma (QGP) that is expected to be produced during the early stage of heavy-ion collisions at CERN Super Proton Synchrotron (SPS) energies [3–10].

Recently, the NA60 Collaboration [11] has measured dileptons from In + In collisions at 158*A* GeV and found that the inverse slope parameter or effective temperature of the transverse mass spectrum of dileptons in the intermediate mass region is lower than that of dileptons at lower masses, which are dominantly of hadronic origin. This might be explained if the dilepton spectrum at invariant masses above 1 GeV is essentially due to partonic channels in the QGP [12–14]. In this case, the softening of the transverse mass spectrum with increasing invariant mass implies that the partonic channels occur dominantly before the collective radial flow has developed.

Because dileptons are emitted over the entire history of the heavy-ion collision, from the initial nucleon-nucleon collisions through the hot and dense phase and to the hadron decays after freeze-out, microscopic covariant transport models are very useful for disentangling the various sources that contribute to the final dilepton spectra seen in experiments. The assumption that the dilepton spectra at masses above 1 GeV might be dominated by radiations from the QGP was supported by studies within the hadron-string dynamics (HSD) transport approach [15], which has shown [16] that the measured dilepton yield at low masses ($M \leqslant$ 1 GeV) can be well explained by dilepton production from hadronic interactions and decays, while there is a discrepancy between the HSD results and the data in the mass region above 1 GeV. The excess seen for $M >$ 1 GeV could not be accounted for by hadronic sources in HSD with or without medium effects and might be interpreted as a signal for the existence of

*olena.linnyk@theo.physik.uni-giessen.de

partonic matter already in heavy-ion collisions at 158A GeV incident energy. Indeed, results from model studies by Dusling and Zahed [17] as well as by Renk and Ruppert [18] have indicated that this excess could be due to partonic channels, i.e., primarily to $q\bar{q}$ annihilation. On the other hand, this dilepton excess has been attributed by Rapp and collaborators to multimeson production channels [19] (denoted shortly as "4π" contribution [20]). These different interpretations of the experimental data are still being extensively debated. In this respect, the physics of dilepton transverse-momentum spectra can be especially relevant [21]. Due to the nonequilibrium nature of heavy-ion collisions, a clarification within a transport approach that incorporates dilepton production from the (nonequillibrium) partonic phase, hadronic decays, and the microscopic secondary hadronic interactions—including the 4π channels—thus appears appropriate.

Another open question to be answered by the microscopic transport calculations is the existence of other "windows" in the phase space for observing dileptons from the QGP over the hadronic sources. The authors of Refs. [8–10] have proposed that sizeable contributions from partonic bremsstrahlung might be seen in the very low mass sector $M < 2m_\pi$. It has been, furthermore, suggested that a substantial thermal yield from the deconfined phase might exist in the invariant mass region between the ϕ and J/Ψ peaks [4], while the spectrum at lower masses should be dominated by meson decays. On the other hand, the calculations [22,23] of the thermal dilepton yield from $q\bar{q}$ annihilation in a blast wave model in comparison to that from a hadronic cocktail, the Drell-Yan mechanism, and the correlated semileptonic decays of open charm have found a possible further region of the phase space for the observation of this thermal source at masses $\approx$0.3–0.6 GeV and low transverse momentum.

The parton-hadron-string dynamics [24,25] (PHSD) transport approach, which incorporates the relevant off-shell dynamics of vector mesons and the explicit partonic phase in the early hot and dense reaction region as well as the dynamics of hadronization, allows for a microscopic study of various dilepton production channels in nonequilibrium matter. The PHSD off-shell transport approach is particularly suitable for this investigation, because it incorporates various scenarios for the modification of vector mesons in a hot and dense medium, seen experimentally in the enhanced production of lepton pairs in the invariant mass range $0.3 \leqslant M \leqslant 0.7$ GeV/c^2. In the present work, we calculate dilepton production from the partonic and hadronic sources within PHSD by including the multimeson channels and the partonic channels besides the usual hadron decay channels. By consistently treating in the same microscopic transport framework both partonic and hadronic phases of the collision system, we are aiming to determine the relative importance of different dilepton production mechanisms and to point out the regions in phase space where partonic channels are dominant.

The paper is organized as follows. In Sec. II, we give a brief description of the PHSD approach. We then describe in Sec. III the partonic sources of dilepton production incorporated in PHSD, and in Sec. IV we describe dilepton production by (in-medium) hadrons and in multimeson processes. In Sec. V, we compare the results of the calculations to the available experimental data. Finally, the conclusions are given in Sec. VI.

II. PHSD TRANSPORT APPROACH

To address dilepton production in a hot and dense medium as created in heavy-ion collisions, we employ an up-to-date relativistic transport model, i.e., PHSD [24,25]. PHSD consistently describes the full evolution of a relativistic heavy-ion collision from the initial hard scatterings and string formation through the dynamical deconfinement phase transition to the quark-gluon plasma as well as hadronization and to the subsequent interactions in the hadronic phase.

In the hadronic sector, PHSD is equivalent to the HSD transport approach [15,26,27] that has been used for the description of pA and AA collisions from GSI Schwerionen Synchrotron (SIS) to BNL Relativisitic Heavy Ion Collider (RHIC) energies and has lead to a fair reproduction of measured hadron abundances, rapidity distributions, and transverse-momentum spectra. In particular, the HSD incorporates off-shell dynamics for vector mesons [28] and a set of vector-meson spectral functions [29] that covers possible scenarios for their in-medium modification.

The transition from the partonic to the hadronic degrees of freedom in PHSD is described by covariant transition rates for the fusion of quark-antiquark pairs to mesonic resonances or three quarks (antiquarks) to baryonic states, i.e., dynamical hadronization. Note that due to the off-shell nature of partons on one hand and the resulting hadrons on the other, the hadronization process obeys all conservation laws (i.e., four-momentum conservation, flavor current conservation) in each event, the detailed balance relations, and the increase in the total entropy S. The transport theoretical description of quarks and gluons in the PHSD is based on a dynamical quasiparticle model (DQPM) for partons matched to reproduce lattice QCD (lQCD) results for a quark-gluon plasma in thermodynamic equilibrium. The DQPM provides the mean fields for gluons and quarks and their effective two-body interactions for the implementation to PHSD.

We briefly recall the basic assumptions of the DQPM (for details about the DQPM and the off-shell transport we refer to Ref. [30]). Following Ref. [31], the dynamical quasiparticle mass (for gluons and quarks) is assumed to be given by the thermal mass in the asymptotic high-momentum regime, which is proportional to the temperature T and a running coupling $g(T/T_c)$ (squared), for which the following parametrization is used:

$$g^2(T/T_c) = \frac{48\pi^2}{(11N_c - 2N_f)\ln[\lambda^2(T/T_c - T_s/T_c)^2]}. \quad (1)$$

Here $N_c = 3$ stands for the number of colors while N_f denotes the number of flavors. The parameters controlling the infrared enhancement of the coupling λ and T_s have been fitted in Ref. [25] to recent lQCD results for the entropy density $s(T)$. An almost perfect reproduction of the energy density $\varepsilon(T)$ and the pressure $P(T)$ from lQCD is achieved as well (cf. Ref. [25]). We note in passing that the strong coupling

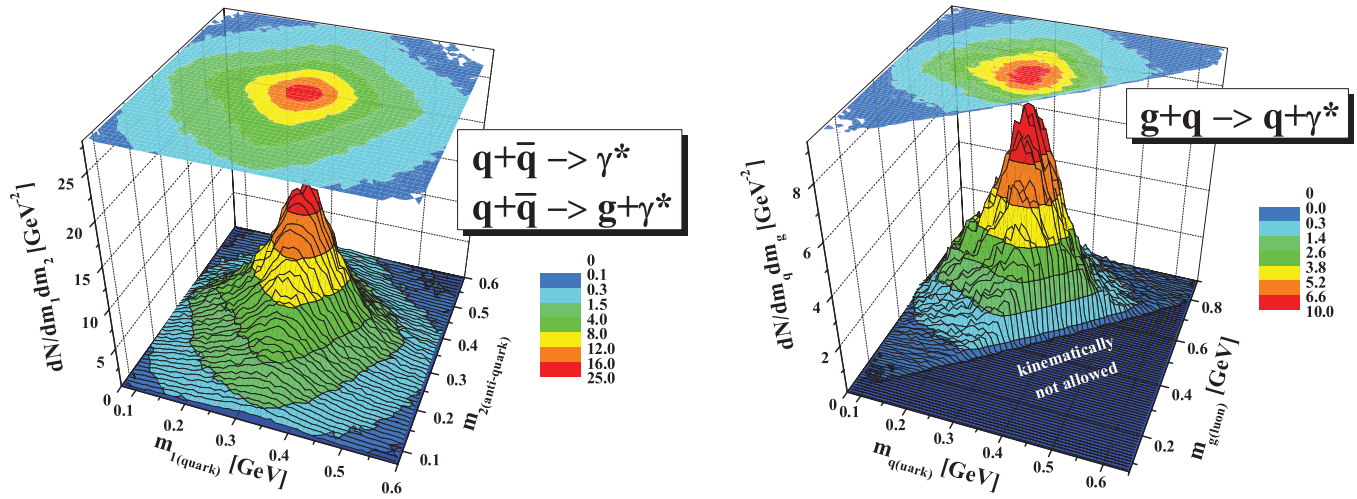

FIG. 1. (Color online) The number of $q + \bar{q}$ (a) and $q + g$ (b) collisions, in which a dilepton pair is produced, in a central In + In reaction at an incident energy of 158A GeV versus the masses of the (quasiparticle) quark and antiquark as resulting from PHSD.

$\alpha_s = g^2/(4\pi)$ in the DQPM is of order unity for temperatures $T \approx T_c$.

In line with Ref. [31], the parton spectral functions are no longer δ functions in the invariant mass squared but are taken as

$$\rho_j(\omega) = \frac{\gamma_j}{E_j}\left(\frac{1}{(\omega - E_j)^2 + \gamma_j^2} - \frac{1}{(\omega + E_j)^2 + \gamma_j^2}\right), \quad (2)$$

separately for quarks and gluons ($j = q, \bar{q}, g$). With the convention $E_j^2(p) = \boldsymbol{p}^2 + M_j^2 - \gamma_j^2$, the parameters M_j^2 and γ_j are directly related to the real and imaginary parts of the retarded self-energy, e.g., $\Pi_j = M_j^2 - 2i\gamma_j\omega$.

The width for gluons and quarks (for vanishing chemical potential μ_q) is adopted in the form

$$\gamma_g(T) = \frac{3g^2T}{8\pi}\ln\left(\frac{2c}{g^2}\right), \quad \gamma_q(T) = \frac{g^2T}{6\pi}\ln\left(\frac{2c}{g^2}\right), \quad (3)$$

where $c = 14.4$ (from Ref. [32]) is related to a magnetic cutoff.

We stress that a nonvanishing width γ is the main difference between the DQPM and conventional quasiparticle models [33]. Its influence is essentially seen in correlation functions, e.g., in the stationary limit of the correlation in the off-diagonal elements of the energy-momentum tensor T^{kl} which defines the shear viscosity η of the medium [32]. Here a sizable width is mandatory to obtain a small ratio of the shear viscosity to entropy density η/s, which results in a roughly hydrodynamical evolution of the partonic system in PHSD [34]. The finite width leads to two-particle correlations, which are taken into account by means of the *generalized*, off-shell transport equations [28] that go beyond the mean-field or Boltzmann approximation [30,35].

The off-shell effect can be seen, for example, in Fig. 1(a) where the number of the $q + \bar{q}$ and $q + g$ collisions—in which a dilepton pair can be formed—is shown as a function of the participating parton masses. The plots have been generated by a simulation in PHSD for a central In + In reaction at an incident energy of 158A GeV. The maximum of the distribution indicates the average pole mass of the quark/gluon, while the width correlates with the average width of their spectral function. The values for the masses and widths are in agreement with those from the DQPM fit to the lattice data for the temperatures in the range $\approx$1–2 T_c.

For an illustration of the quark and gluon interactions in a heavy-ion collision as generated in PHSD, we show in Fig. 2 the number of $q + \bar{q}$ (solid line) and $q + g$ (dashed line) collisions that can create dilepton pairs per event in a central In + In reaction at an incident energy of 158A GeV versus the invariant energy $\sqrt{s}$ of the elementary partonic collision. One can see that the tails of the collision distributions calculated in the PHSD transport are almost exponential, thus

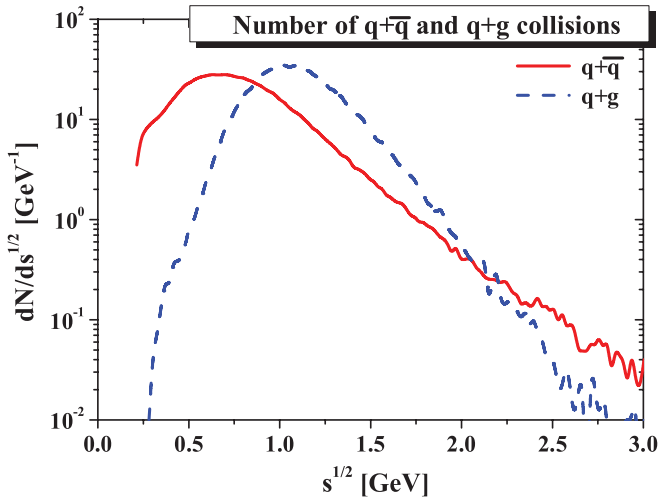

FIG. 2. (Color online) Number of parton collisions per event in a central In + In reaction at an incident energy of 158A GeV versus the invariant energy $\sqrt{s}$ of the elementary partonic collision as simulated in PHSD. The number of $q + \bar{q}$ collisions is given by the solid (red) line while that of $q + g$ collisions is given by the dashed (blue) line.

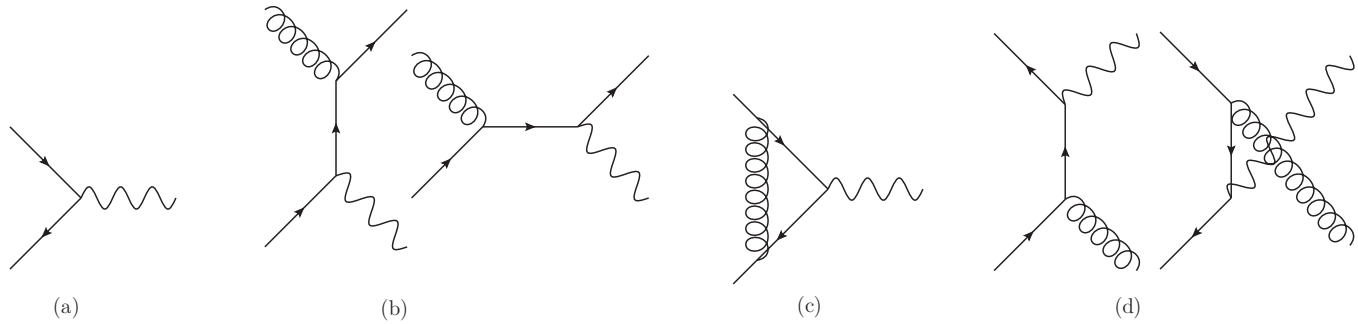

FIG. 3. Diagrams contributing to dilepton production from the QGP: (a) Drell-Yan mechanism, (b) gluon-Compton scattering (GCS), (c) vertex correction, and (d) gluon bremsstrahlung (NLODY), where virtual photons (wavy lines) split into lepton pairs, spiral lines denote gluons, and arrows denote quarks. In each diagram the time runs from left to right.

close to thermal. On the other hand, the collisions at very low $\sqrt{s}$ are suppressed. This "threshold effect" is due to the finite masses of the dynamical quarks, antiquarks, and gluons. Additionally, one notices that the threshold is not sharp because of the rather broad spectral functions (and therefore broad mass distributions) of the colliding partons.

III. PARTONIC SOURCES OF DILEPTONS IN PHSD

In the scope of the one- and two-particle interactions, dilepton radiation by the constituents of the strongly interacting QGP proceeds via the elementary processes illustrated in Figs. 3 and 4: the basic Born $q + \bar{q}$ annihilation mechanism, gluon-Compton scattering ($q + g \to \gamma^* + q$ and $\bar{q} + g \to \gamma^* + \bar{q}$), and quark + antiquark annihilation with gluon bremsstrahlung in the final state ($q + \bar{q} \to g + \gamma^*$), virtual quark decay ($q \to q + g + \gamma^*$), and virtual gluon decay ($g \to q + \bar{q} + \gamma^*$). In the on-shell approximation, one uses perturbative QCD cross sections for the processes listed above. However, in the strongly interacting QGP the gluon and quark propagators differ significantly from the noninteracting propagators. Accordingly, the cross sections for dilepton production in the partonic channels have been calculated in Ref. [36] in the DQPM model that had been fitted to lattice QCD results in thermal equilibrium before Ref. [32].

The importance of finite mass corrections to the perturbative cross sections has been stressed in Ref. [36]. It was shown that the finite quark and gluon masses can modify the magnitude as well as the M dependence and p_T dependence of the cross sections of the processes in Fig. 1 compared to the perturbative results for massless partons (cf. Figs. 3 and 4 of Ref. [36]). The modifications are large at lower M^2 and at the edges of the phase space. It was shown that the most prominent effect of the quark masses on the dimuon production cross sections in the Born mechanism ($q + \bar{q} \to \gamma^*$) was a sharp threshold value for the invariant mass of the dilepton pair $M_{\min} = m_1 + m_2$. On the other hand, the finite masses of the quark and antiquark produce additional higher-twist corrections to the cross section, which decrease with increasing M^2, so that the off-shell cross sections approach the leading twist—on-shell—result in the limit of high dilepton masses. In Fig. 4 of Ref. [36], an analogous comparison for the $2 \to 2$ process $q + \bar{q} \to \gamma^* + g$ was shown by plotting the off-shell (i.e., with finite masses for the quarks and gluons) cross section for the quark annihilation with gluon bremsstrahlung in the final state at various values of the quark and gluon off-shellnesses (masses) and the corresponding on-shell result. As found in Ref. [36], the maximum pair mass shifts to a lower value (to produce a massive gluon in the final state). For the rest of the M values, the effect of the quark and gluon masses is about 50%. For $m_{q/g} \to 0$, the cross section approaches the leading twist pQCD result.

The question of the effect of a finite parton width—which parametrizes the effect of their interaction rate and correlation, including multiple scattering—on dilepton rates in heavy-ion collisions was addressed in Ref. [36] by convoluting the off-shell cross sections with phenomenological spectral functions $A(m_q)$ and $A(m_g)$ for the quarks and gluons in the quark-gluon plasma and with parton distributions in a heavy-ion collision similar to those of Fig. 2 in the present paper. The finite width of the quasiparticles was found to have a sizable effect on the dilepton production rates. In particular, the threshold of the Drell-Yan contribution was washed out. Also, the shape and magnitude of the $2 \to 2$ processes ($q + \bar{q} \to g + \gamma^*$ and $q + g \to q + \gamma^*$) were modified. We further observed that the

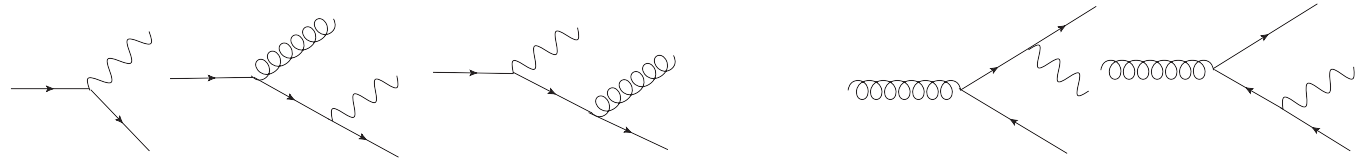

FIG. 4. Diagrams contributing to dilepton production by virtual quasiparticles in addition to those presented in Fig. 3. First three diagrams: The decay of a virtual quark. The last two diagrams: The decay of a virtual gluon. Virtual photons (wavy lines) split into lepton pairs, spiral lines denote gluons, and arrows denote quarks.

contribution of the gluon-Compton process $q + g \to q + \gamma^*$ to the rates was small compared to that of $q + \bar{q}$ annihilations.

In the present work, we implement the cross sections obtained in Ref. [36] into the PHSD transport approach in the following way. Whenever the quark-antiquark, quark-gluon, and antiquark-gluon collisions occur in the course of the Monte Carlo simulation of the partonic phase in PHSD, a dilepton pair can be produced according to the off-shell cross sections [36], which depend, in addition to the virtualities of the partons involved, on the energy density in the local cell, in which the collision takes place. The local energy density governs the widths of the quark and gluon spectral functions as well as the strong coupling [cf. Eqs. (1) and (3) that depend on temperature T, which in turn is uniquely related to the energy density by the lattice QCD equation of state]. Numerically, one finds from a PHSD simulation of a heavy-ion collision at SPS energies that the running coupling α_S in the partonic phase is often of order $O(1)$ and thus the contribution of the higher-order bremsstrahlung diagram is compatible in magnitude to the Born term.

IV. HADRONIC SOURCES OF DILEPTONS IN PHSD

In the hadronic sector, PHSD is equivalent to the HSD transport approach [15,26,27]. The implementation of the hadronic decays into dileptons (π-, η-, η'-, ω-, Δ-, a_1-Dalitz, $\rho \to l^+l^-$, $\omega \to l^+l^-$, $\phi \to l^+l^-$) in HSD (and PHSD) is described in detail in Refs. [16,29]. For the treatment of the leptonic decays of open charm mesons and charmonia we refer to Refs. [37,38]. In the present paper, we extend the hadronic sources for dilepton production to include secondary multimeson interactions by incorporating the channels $\pi\omega \to l^+l^-$, $\pi a_1 \to l^+l^-$, and $\rho\rho \to l^+l^-$.

The dilepton production by a (baryonic or mesonic) resonance R decay in HSD and PHSD can be schematically presented in the following way:

$$BB \to RX \tag{4}$$

$$mB \to RX \tag{5}$$

$$R \to e^+e^-X, \tag{6}$$

$$R \to mX,\ m \to e^+e^-X, \tag{7}$$

$$R \to R'X,\ R' \to e^+e^-X, \tag{8}$$

i.e., in a first step a resonance R might be produced in baryon-baryon (BB) or meson-baryon (mB) collision, Eqs. (4) and (5), respectively. Then this resonance can couple to dileptons directly, Eq. (6) (e.g., Dalitz decay of the Δ resonance: $\Delta \to e^+e^-N$), or decay to a meson m (+baryon) or in Eq. (7) produce dileptons via direct decays (ρ, ω) or Dalitz decays (π^0, η, ω). The resonance R might also decay into another resonance R' (8) which later produces dileptons via Dalitz decay. Note that in the combined model the final particles—which couple to dileptons—can be produced also via nonresonant mechanisms, i.e., "background" channels at low and intermediate energies or string decay at high energies. Further channels contributing to low-mass dilepton production are pion-pion bremsstrahlung or (in general) meson-meson bremsstrahling [9,10]. These channels essentially contribute to the dilepton spectrum at invariant masses below about $2m_\pi$ and are also hard to disentangle from the dominant π^0- and η-Dalitz decays. Because in this work we address $\mu^+\mu^-$ pair production with a threshold of 211 MeV we have discarded an explicit calculation of these channels although an inclusion of the channels with the cross sections from Refs. [9,10] is straight forward.

A. In-medium modification of vector mesons

While the properties of hadrons are rather well known in free space (embedded in the nonperturbative QCD vacuum), the masses and lifetimes of hadrons in a baryonic and/or mesonic environment are the subject of current research that aims at achieving a better understanding of the strong interaction and the nature of confinement. For example, a broadening of the vector mesons can be understood as a shortening of the lifetime of the vector mesons ρ, ω, and ϕ in the medium. In this context the modification of hadron properties in nuclear matter are of fundamental interest (cf. Refs. [39–43]), because QCD sum rules [40,41,44] as well as QCD inspired effective Lagrangian models [39,42,45,46] predict significant changes, e.g., in the properties of the vector mesons (ρ, ω, and ϕ) with the nuclear density ρ_N and/or temperature T [15,47–49].

A modification of the properties of vector mesons in the nuclear medium was first seen experimentally in the enhanced production of lepton pairs above known sources in nucleus-nucleus collisions at SPS energies [50,51]. As proposed in Refs. [52,53], the observed enhancement in the invariant mass range $0.3 \leqslant M \leqslant 0.7$ GeV/c^2 might be due to a shift of the ρ-meson mass following the Brown-Rho scaling [39] or the Hatsuda-Lee sum rule prediction [40]. The microscopic transport studies in Refs. [15,26,54,55] for these systems have given support for this interpretation. On the other hand, more conventional approaches that describe a melting of the ρ meson in the medium due to the strong hadronic coupling (along the lines of Refs. [45,46]) have also been found to be compatible with the early data from the CERES Collaboration [47,54,56,57]. This ambiguous situation has been clarified to some extent in 2006 by the NA60 Collaboration because the invariant mass spectra for $\mu^+\mu^-$ pairs from In + In collisions at 158A GeV favored the "melting" scenario [11]. Also, the later data from the CERES Collaboration (with enhanced mass resolution) [58] showed a preference for the "melting ρ" picture.

The various models, which predict a change of the hadronic spectral functions in the (hot and dense) nuclear medium, may be classified into two different categories: (i) a broadening of the spectral function or (ii) a mass shift of the vector mesons with density and/or temperature. In view of many-body dynamics, both modifications should be studied simultaneously as well [1,59]. Thus we explore in the present study three possible scenarios with respect to the low-mass dilepton spectrum which essentially address all possible properties of the ρ meson: (1) a broadening of the ρ spectral function, (2) a mass shift, and (3) a broadening plus a mass shift.

We incorporate the effect of collisional broadening of the vector-meson spectral functions (as in Refs. [60,61]) by using

for the vector-meson width:

$$\Gamma_V^*(M, |\vec{p}|, \rho_N) = \Gamma_V(M) + \Gamma_{\rm coll}(M, |\vec{p}|, \rho_N). \quad (9)$$

Here $\Gamma_V(M)$ is the total width of the vector mesons ($V = \rho, \omega$) in the vacuum. The collisional width in Eq. (9) is approximated as

$$\Gamma_{\rm coll}(M, |\vec{p}|, \rho_N) = \gamma\ \rho_N \langle v\ \sigma_{VN}^{\rm tot} \rangle \approx\ \alpha_{\rm coll}\ \frac{\rho_N}{\rho_0}. \quad (10)$$

Here $v = |\vec{p}|/E$, $\vec{p}$, and E are the velocity, three-momentum, and energy of the vector meson in the rest frame of the nucleon current and $\gamma^2 = 1/(1 - v^2)$. Furthermore, ρ_N is the nuclear density and $\sigma_{VN}^{\rm tot}$ is the meson-nucleon total cross section.

To simplify the actual calculations for dilepton production, the coefficient $\alpha_{\rm coll}$ has been extracted in the PHSD transport calculations from the vector-meson collision rate in In + In reactions at 158A GeV as a function of the density ρ_N. In case of the ρ meson the collision rate is dominated by the absorption channels $\rho N \to \pi N$ or $\rho N \to \Delta\pi \to \pi\pi N$. Also the reactions $\rho + \pi \leftrightarrow a_1$ are incorporated. The numerical results for $\Gamma_{\rm coll}(\rho_N)$ then have been divided by ρ_N/ρ_0 to fix the coefficient $\alpha_{\rm coll}$ in Eq. (10). We obtain $\alpha_{\rm coll} \approx 150$ MeV for the ρ mesons and $\alpha_{\rm coll} \approx 70$ MeV for the ω mesons, which are values that are consistent with those of Ref. [62]. In this way the average effects of collisional broadening are incorporated in accordance with the transport calculations and allow for an explicit representation of the vector-meson spectral functions versus the nuclear density as demonstrated in Ref. [29].

To explore the observable consequences of vector-meson mass shifts at finite nuclear density, the in-medium vector-meson pole masses are modeled (optionally) according to the Hatsuda-Lee sum rule prediction [40] or the Brown-Rho scaling [39] as

$$M_0^*(\rho_N) = \frac{M_0}{(1 + \alpha\rho_N/\rho_0)}, \quad (11)$$

where ρ_N is the nuclear density at the resonance decay position $\vec{r}$, $\rho_0 = 0.16$ fm^{-3} is the normal nuclear density, and $\alpha \simeq 0.16$ for the ρ meson and $\alpha \simeq 0.12$ for the ω meson [62]. The parametrization (11) may be employed also at much higher collision energies and one does not have to introduce a cutoff density to avoid negative pole masses. Note that Eq. (11) is uniquely fixed by the "customary" expression $M_0^*(\rho_N) \approx M_0(1 - \alpha\rho_N/\rho_0)$ in the low-density regime.

The spectral function of the vector meson V for the mass M at baryon density ρ_N is taken in the Breit-Wigner form:

$$A_V(M, \rho_N) = C_1 \frac{2}{\pi} \frac{M^2 \Gamma_V^*(M, \rho_N)}{\left[M^2 - M_0^{*^2}(\rho_N)\right]2 + [M\Gamma_V^*(M, \rho_N)]^2}. \quad (12)$$

The factor C_1 is fixed by the normalization condition for arbitrary ρ_N:

$$\int_{M_{\rm min}}^{M_{\rm lim}} A_V(M, \rho_N)\, dM = 1, \quad (13)$$

where $M_{\rm lim} = 2$ GeV is chosen as an upper limit for the numerical integration. The lower limit for the vacuum spectral function corresponds to the two-pion decay, $M_{\rm min} = 2m_\pi$, whereas for the in-medium collisional broadening case $M_{\rm min} = 2m_e \to 0$, with m_e denoting the electron mass. M_0^* is the pole mass of the vector-meson spectral function which is $M_0^*(\rho_N = 0) = M_0$ in vacuum, but may be shifted in the medium for the dropping mass scenario according to Eq. (11). The resulting spectral functions for the ρ and ω mesons are displayed in Fig. 2 of Ref. [29].

With increasing nuclear density ρ_N elastic and inelastic interactions of the vector mesons shift strength to low invariant masses. In the collisional broadening scenario we find a dominant enhancement of strength below the pole mass for the ρ meson while the ω-meson spectral function is drastically enhanced in the low- and high-mass region with density (on expense of the pole-mass regime). In the "dropping mass + collisional broadening" scenario both vector mesons dominantly show a shift of strength to low invariant masses with increasing ρ_N. Qualitatively similar pictures are obtained for the ϕ meson but quantitatively smaller effects are seen due to the lower effect of mass shifts and a substantially reduced ϕN cross section which is a consequence of the $s\bar{s}$ substructure of the ϕ meson.

Note that, just like the HSD, the PHSD incorporates the *off-shell propagation* for vector mesons—according to Ref. [28]. In the off-shell transport, the hadron spectral functions change dynamically during the propagation through the medium and evolve toward the on-shell spectral functions in the vacuum. The PHSD off-shell transport approach is particularly suitable for investigating the different scenarios for the modification of vector mesons in a hot and dense medium. As demonstrated in Ref. [29], the off-shell dynamics is important for resonances with a rather long lifetime in the vacuum but a strongly decreasing lifetime in the nuclear medium (especially ω and ϕ mesons) and also proves vital for the correct description of dilepton decays of ρ mesons with masses close to the two-pion decay threshold. For a detailed description of the off-shell dynamics we refer the reader to Refs. [16,28,29,35].

B. Multimeson channels of dilepton production

The dilepton excess yield in In + In collisions at 158A GeV incident energy for $M > 1$ GeV/c^2 was found to be dominated by partonic sources within the dynamical studies of Renk and Ruppert [18] and Dusling and Zahed [17]. On the other hand, the model of van Hees and Rapp [19] suggested dominance of hadronic sources dubbed "4π channels." To clarify this question, we have incorporated in the PHSD the 4π channels for dilepton production on a microscopic level rather than assuming thermal dilepton production and incorporating a parametrization for the inverse reaction $\mu^+ + \mu^- \to 4\pi's$ by employing detailed balance as in Refs. [20,63].

By studying the electromagnetic emissivity (in the dilepton channel) of the hot hadron gas, it was shown in Refs. [64,65] that the dominating hadronic reactions contributing to the dilepton yield at the invariant masses above the ϕ peak are the two-body reactions, i.e., $\pi + \rho$, $\pi + \omega$, $\rho + \rho$, and $\pi + a_1$. This conclusion was supported by the subsequent study in a hadronic relativistic transport model [66]. Therefore, we implement the above-listed two-meson dilepton production channels in the PHSD approach. In addition, some higher vector mesons (ρ', etc.) are tacitly included by using phenomenological form factors adjusted to data.

We determine the cross sections for the mesonic interactions with dileptons in the final state using an effective Lagrangian approach, following the works of Refs. [64,66]. The dilepton production cross section is given by the product of a form factor and the square of a scattering amplitude,

$$\frac{d\sigma}{dt} = \frac{1}{64\pi s}\frac{1}{|p_{\text{c.m.}}|^2}|\bar{M}|^2|F(M)|^2, \tag{14}$$

where

$$p_{\text{c.m.}} = \sqrt{(s-(m_1+m_2)^2)(s-(m_1-m_2)^2)}/2\sqrt{s} \tag{15}$$

is the center-of-mass momentum of the colliding hadrons with the masses m_1 and m_2, and $|\bar{\mathcal{M}}|^2$ can be written as

$$|\bar{\mathcal{M}}|^2 = 4\left(\frac{4\pi\alpha}{q^2}\right)^2 L_{\mu\nu}H^{\mu\nu}, \tag{16}$$

with $q = p_1 + p_2 = p_3 + p_4$ and the fine structure constant α. In Eq. (16), $L_{\mu\nu}$ is the leptonic tensor given by

$$L^{\mu\nu} = p_3^\mu p_4^\nu + p_4^\mu p_3^\nu - g^{\mu\nu}(p_3p_4 + m_l^2), \tag{17}$$

while $H^{\mu\nu}$ is a hadronic tensor for the reaction.

The hadronic tensor $H^{\mu\nu}$ for the reaction $\pi^+ + \pi^- \to e^+ + e^-$ is given by

$$H^{\mu\nu} = (p_2^\mu - p_1^\mu)(p_2^\nu - p_1^\nu), \tag{18}$$

which leads to the well-known result for the $\pi\pi$ annihilation cross section,

$$\sigma_\pi(s) = \frac{4\pi\alpha^2}{3s}|F_\pi|^2\sqrt{1-\frac{4m_\pi^2}{s}}\left(1-\frac{4m_l^2}{M^2}\right)\left(1+\frac{2m_l^2}{M^2}\right), \tag{19}$$

where M is the mass of the lepton pair and m_l is the mass of the lepton. The electromagnetic form factor $|F_\pi(M)|^2$ plays an important role in this process, providing empirical support for the vector-meson dominance: the pion electromagnetic form factor is dominated by the $\rho(770)$ meson. In Ref. [67], Gale and Kapusta proposed the form

$$|F_\pi(M)|^2 = \frac{m_r^4}{\left(M^2 - m_r'^2\right)^2 + (m_r\Gamma_r)^2}, \tag{20}$$

where $m_r = 0.775$ GeV, $m_r' = 0.761$ GeV, and $\Gamma_r = 0.118$ GeV. The expressions (18)–(20) will be used for an estimate of the dilepton production in pion-pion channel in the scope of the thermal model in Sec. V; note however that in the actual transport calculations in Sec. VI a realistic density-dependent spectral function for the intermediate rho is used instead.

According to Ref. [68], the cross section for $\pi\rho$ annihilation is given by

$$\sigma(\pi^+\rho^- \to l\bar{l}) = \frac{2\pi\alpha^2 p_{\text{c.m.}}}{9M}|F_{\pi\rho}|^2\left(1-\frac{4m_l^2}{M^2}\right)\left(1+\frac{2m_l^2}{M^2}\right). \tag{21}$$

Note that the cross section (21) is evaluated in the narrow-width approximation for illustration purposes only. This simplification is not used in the actual transport calculation. The electromagnetic form factor $|F_{\pi\rho}(M)|^2$ can then be determined by analyzing the experimental data for $e^+e^- \to \pi^+\pi^-\pi^0$. In Ref. [68], three isoscalar vector mesons, $\phi(1020)$, $\omega(1420)$, and $\omega(1670)$ were found to be important to fit the experimental data, namely,

$$F_{\pi\rho}(M) = \sum_V \left(\frac{g_{V\pi\rho}}{g_V}\right)\frac{e^{i\phi_V}m_V^2}{\left(m_V^2 - M^2\right) - im_V\Gamma_V}. \tag{22}$$

Here the summation runs over the three vector mesons listed above. While the coupling constants g_ϕ and $g_{\phi\pi\rho}$ can be determined from the measured widths, the coupling constants for the other two mesons and the relative phases were determined by a fit to the experimental data of Refs. [69,70]. These coupling constants were extracted from the latest data of the DM2 Collaboration [71] and the ND Collaboration [72]. The parameters are listed in Ref. [68]. The comparison of the fit to the experimental data is shown in Fig. 5(a).

The cross section for lepton pair production in pion-ω annihilation is given by [66]

$$\sigma(\pi^0\omega \to l\bar{l}) = \frac{4\pi\alpha^2 p_{\text{c.m.}}}{9M}|F_{\pi\omega}|^2\left(1-\frac{4m_l^2}{M^2}\right)\left(1+\frac{2m_l^2}{M^2}\right). \tag{23}$$

The form factor can be parametrized as follows in terms of three isovector ρ-like vector mesons, $\rho(770)$, $\rho(1450)$, and $\rho(1700)$,

$$F_{\pi\omega}(M) = \sum_V \left(\frac{g_{V\pi\omega}}{g_V}\right)\frac{e^{i\phi_V}m_V^2}{\left(m_V^2 - M^2\right) - im_V\Gamma_V}. \tag{24}$$

Here the summation runs over the three ρ-like resonances listed above. The parameters used are $m_{r1} = 0.77$ GeV, $m_{r2} = 1.45$ GeV, $m_{r3} = 1.7$ GeV, $\Gamma_{r1} = 0.118$ GeV, $\Gamma_{r2} = 0.25$ GeV, $\Gamma_{r3} = 0.22$ GeV, $A_{r1} = 0.85$, $A_{r2} = -0.077$, and $A_{r3} = 0.034$, where $A_V = (g_{V\pi\omega}/g_V)\exp\{i\phi_V\}$. The comparison with the experimental data of the ND [72] and ARGUS Collaborations [73] is shown in Fig. 5(b).

Additionally, we consider the reactions $\pi a_1 \to l\bar{l}$ and $\rho\rho \to l\bar{l}$, which are effectively four-pion processes. Using the Lagrangian for the πa_1 interaction,

$$\mathcal{L}_{\pi a_1\gamma *} = gea^\mu[(\partial_\nu A_\mu)(\partial^\nu\pi) - (\partial_\mu A^\nu)(\partial_\nu\pi)], \tag{25}$$

one obtains for the cross section of the $\pi a_1 \to l\bar{l}$ process

$$\begin{aligned}
&\sigma(\pi a_1 \to l\bar{l}) \\
&= \frac{\pi\alpha^2 g^2 M}{3p_{\text{c.m.}}}\left(1-\frac{4m_l^2}{M^2}\right)\left(1+\frac{2m_l^2}{M^2}\right) \\
&\quad\times\left\{\frac{1}{4}\left(1-\frac{m_{a1}^2}{M^2}\right)\left[1+\frac{2}{m_{a1}^2}\left(\frac{5p_{\text{c.m.}}^2}{12}+\frac{m_{a1}^2}{2}\right)\right]\right. \\
&\quad+\left(1-\frac{m_{a1}^2}{M^2}\right)\left\{-\frac{1}{2}\left(1-\frac{m_{a1}^2}{M^2}\right)+\frac{\sqrt{p_{\text{c.m.}}^2+m_\pi^2}}{M}\right. \\
&\quad-\frac{M^2}{2m_{a1}^2}\left(1+\frac{m_{a1}^2}{M^2}\right)\left[\frac{p_{\text{c.m.}}^2}{6M^2}-\frac{1}{2}\left(1-\frac{m_{a1}^2}{M^2}\right)\right. \\
&\quad\left.\left.+\frac{\sqrt{p_{\text{c.m.}}^2+m_{a1}^2}\sqrt{p_{\text{c.m.}}^2+m_\pi^2}}{M^2}\right]\right\} \\
&\quad\left.+\frac{5p_{\text{c.m.}}^2}{6M^2}\left[\frac{\left(M^2+m_{a1}^2\right)^2}{4m_{a1}^2M^2}-1\right]\right\}|F_{\pi a_1}|^2,
\end{aligned} \tag{26}$$

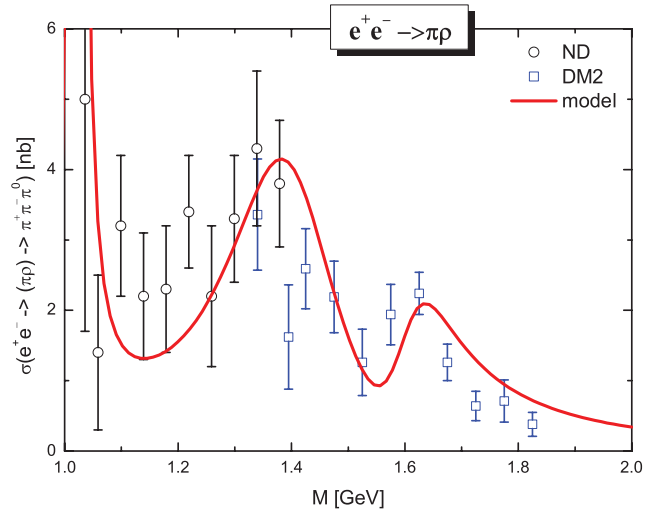

(a)

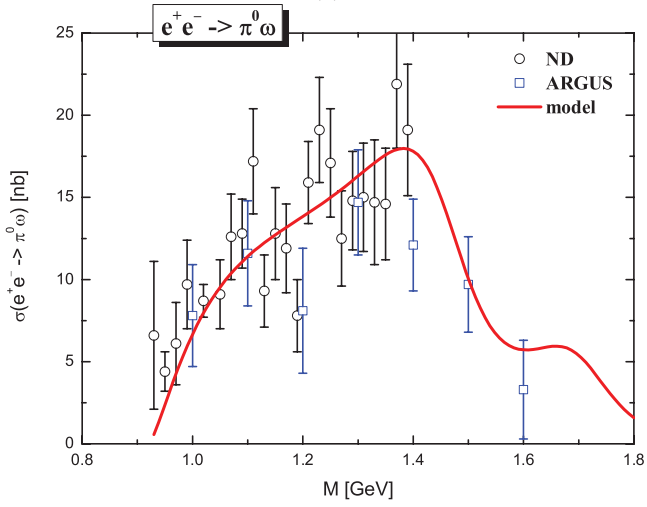

(b)

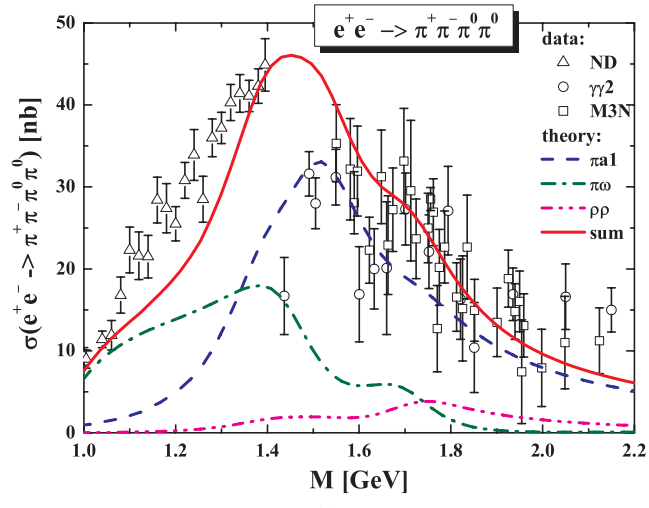

(c)

FIG. 5. (Color online) (a) Cross sections for the reactions $e^+e^- \to \pi + \rho$ (a) and $e^+e^- \to \pi + \omega$ (b) in our model versus the experimental data. Panel (c) gives the measured cross section of the $e^+e^- \to \pi^+\pi^-\pi^0\pi^0$ reaction versus the sum of the model cross sections for $e^+e^- \to \pi + \omega$, $e^+e^- \to \pi + a_1$, and $e^+e^- \to \rho + \rho$.

where the value of the coupling constant $g = (g_\rho/f_\rho)$ is adjusted so that the experimentally measured radiative decay widths are reproduced.

We obtain the hadronic tensor $H^{\mu\nu}$ for the reaction $\rho^+\rho^- \to e^+e^-$ by generalizing the formula of Ref. [64] to explicitly take into account the broad spectral functions of the colliding ρ mesons:

$$\begin{aligned} H^{\mu\nu} = {} & h_\rho^{\mu\alpha\beta} h^{\nu}_{\rho\alpha\beta} - h_\rho^{\mu\alpha\beta} p_{1\beta} h^{\nu\gamma}_{\rho\alpha} p_{1\gamma}/m_{\rho 1}^2 \\ & - h_\rho^{\mu\alpha\beta} p_{2\alpha} h^{\nu\gamma}_{\rho\beta} p_{2\gamma}/m_{\rho 2}^2 \\ & + h_\rho^{\mu\alpha\beta} p_{1\beta} p_{2\alpha} h_\rho^{\nu\gamma\delta} p_{2\gamma} p_{1\delta} \big/ \left(m_{\rho 1}^2 m_{\rho 2}^2\right), \end{aligned} \tag{27}$$

with

$$h_\rho^{\mu\alpha\beta} = \left(p_2^\mu - p_1^\mu\right) g^{\alpha\beta} + \left(q^\alpha - p_2^\alpha\right) g^{\beta\mu} + \left(p_1^\beta - q^\beta\right) g^{\mu\alpha}. \tag{28}$$

In this case, the hadronic tensor depends on (generally different) masses of the colliding particles $m_{\rho 1}$ and $m_{\rho 2}$. In the actual transport calculations, $m_{\rho i}$ are distributed according to the dynamical spectral functions. Using Eqs. (14)–(16) and (27) we obtain the following cross section as a function of M, $m_{\rho 1}$, and $m_{\rho 2}$:

$$\begin{aligned} & \sigma(\rho\rho \to l^+l^-) \\ & = \frac{\pi\alpha^2 |F_{\rho\rho}|^2}{120 m_{\rho 1}^2 m_{\rho 2}^2 M^5 p_{\text{c.m.}}} \left[9m_{\rho 1}^8 + 18 m_{\rho 1}^6 \left(3m_{\rho 2}^2 - 2M^2\right)\right. \\ & \quad + \left(m_{\rho 2}^2 - M^2\right)^2 \left(819 m_{\rho 2}^4 + 632 m_{\rho 2}^2 M^2 - 11 M^4\right) \\ & \quad - 2m_{\rho 1}^2 \left(363 m_{\rho 2}^6 + 32 m_{\rho 2}^4 M^2 + 327 m_{\rho 2}^2 M^4 - 2M^6\right) \\ & \quad \left. + m_{\rho 1}^4 \left(-156 m_{\rho 2}^4 + 266 m_{\rho 2}^2 M^2 + 34 M^4\right)\right], \end{aligned} \tag{29}$$

which reduces in the narrow width approximation to

$$\begin{aligned} & \sigma(\rho\rho \to l^+l^-) \\ & = \frac{\pi\alpha^2 |F_{\rho\rho}|^2}{60 m_\rho^4 M^3 \sqrt{M^2 - 4m_\rho^2}} \\ & \quad \times \left(840 m_\rho^6 + 1076 m_\rho^4 M^2 - 658 m_\rho^2 M^4 + 11 M^6\right). \end{aligned} \tag{30}$$

The form factors $|F_{\pi a_1}|^2$ and $|F_{\rho\rho}|^2$ can be determined by analyzing the $e^+e^- \to \pi^+\pi^-\pi^+\pi^-$ and $e^+e^- \to \pi^+\pi^-\pi^0\pi^0$ data. We determine $|F_{\pi a_1}(M)|^2$ from experimental data for $e^+e^- \to \pi^+\pi^-\pi^+\pi^-$ from the $\gamma\gamma 2$ Collaboration [74], the M3N Collaboration [75], and the ND Collaboration [72]. Further constraints on $|F_{\pi a_1}|^2$ and the determination of $|F_{\rho\rho}|^2$ were provided by the experimental data for $e^+e^- \to \pi^+\pi^-\pi^0\pi^0$, which can come from $\pi\omega$, πa_1, and $\rho\rho$ intermediate states. Our form factors are

$$F_{\pi a_1}(M) = \sum_V \left(\frac{g_{V\pi a_1}}{g_V}\right) \frac{e^{i\phi_V} m_V^2}{\left(m_V^2 - M^2\right) - i m_V \Gamma_V}, \tag{31}$$

with $m_{r1} = 0.77$ GeV, $m_{r2} = 1.45$ GeV, $m_{r3} = 1.7$ GeV, $\Gamma_{r1} = 0.118$ GeV, $\Gamma_{r2} = 0.25$ GeV, $\Gamma_{r3} = 0.235$ GeV, $A_{r1} = 0.05$, $A_{r2} = 0.58$, and $A_{r3} = 0.027$, and

$$F_{\rho\rho}(M) = \sum_V \left(\frac{g_{V\rho\rho}}{g_V}\right) \frac{e^{i\phi_V} m_V^2}{\left(m_V^2 - M^2\right) - i m_V \Gamma_V}, \tag{32}$$

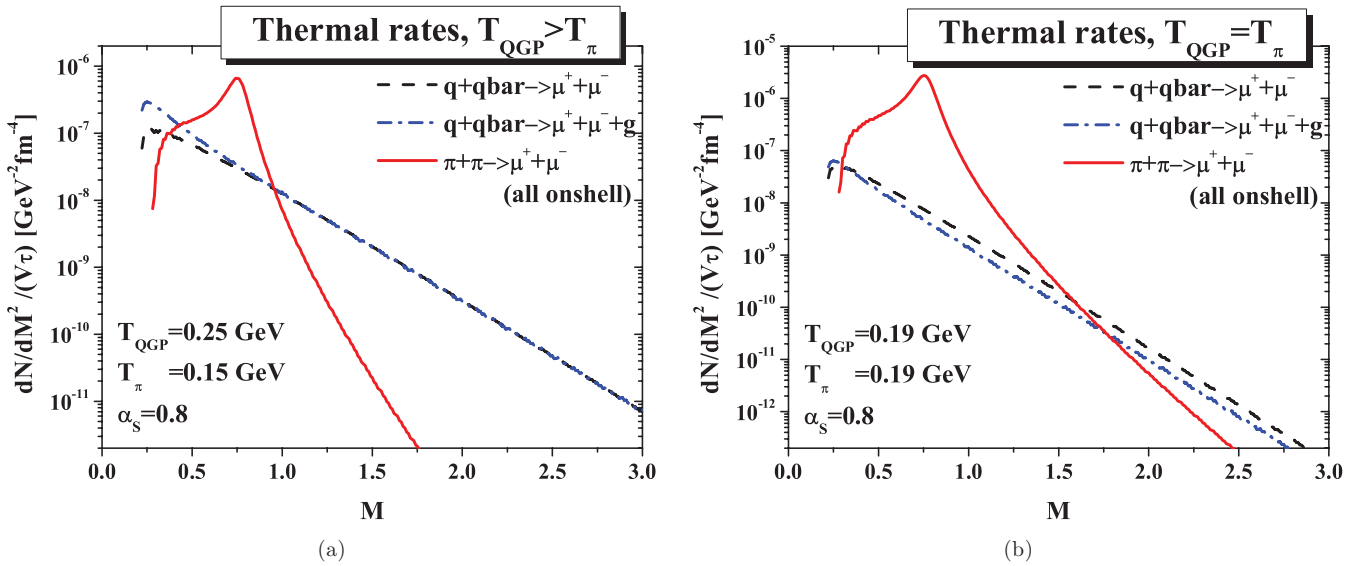

FIG. 6. (Color online) Rates of dileptons created in $q + \bar{q}$ and $\pi + \pi$ annihilations within a thermalized gas of quarks with temperature $T_{\rm QGP}$ and pions with temperature T_π. (a) $T_{\rm QGP} = 250$ MeV, $T_\pi = 150$ MeV; (b) $T_{\rm QGP} = T_\pi = 190$ MeV.

with $m_{r1} = 0.77$ GeV, $m_{r2} = 1.45$ GeV, $m_{r3} = 1.7$ GeV, $\Gamma_{r1} = 0.118$ GeV, $\Gamma_{r2} = 0.237$ GeV, $\Gamma_{r3} = 0.235$ GeV, $A_{r1} = 0.05$, $A_{r2} = 0.05$, and $A_{r3} = 0.02$. The comparison to the data is shown in Fig. 5(c).

Let us summarize that to fix the form factors in the cross sections for dilepton production by the interaction of $\pi + \rho$, $\pi + \omega$, $\rho + \rho$, and πa_1 we use the measurements in the detailed-balance-related channels: $e^+e^- \to \pi + \rho$, $e^+e^- \to \pi + \omega$, $e^+e^- \to \rho + \rho$, and $e^+e^- \to \pi + a_1$. Note that we fitted the form factors while taking into account the widths of the ρ and a_1 mesons in the final state by convoluting the cross sections with the (vacuum) spectral functions of these mesons in line with Ref. [76] (using the parametrizations of the spectral functions as implemented in HSD and described in Ref. [77]). In Fig. 5 we present the resulting cross sections, which are related by detailed balance to the ones we implemented in PHSD.

V. DILEPTON RATES IN THERMAL EQUILIBRIUM

Before proceeding to the results of the transport calculations and the comparison to data, we dedicate this section to a study of the dilepton spectrum qualitatively in a thermal model. In Fig. 6, the dilepton production rates in thermal equilibrium are presented. We assume here that the system evolves through a thermalized system of quark in the hot initial stage of the heavy-ion collision and through the state of a high-density hadron gas in the later phase of the collision.

The main elementary process of dilepton production in a hadron gas is the pion annihilation into dileptons, mediated through vector-meson dominance by the ρ meson ($\pi + \pi \to \rho \to \gamma^* \to l^+ + l^-$) and controlled by the pole at the ρ mass of the pion electromagnetic form factor. For the pion annihilation, we use the standard cross section as, e.g., in Ref. [64], and the Breit-Wigner form factor with the pole mass and width of the ρ meson.

In the partonic sector, the main sources of the dileptons are the reactions of quark-antiquark annihilation with the production of the virtual photon. Considering the temperatures and baryon densities relevant for the SPS energies, we expect in PHSD the contribution of the processes involving gluons to be small compared to the leading $q + \bar{q}$ mechanism of dilepton production (note, however, that at higher energies, such as those of the RHIC and the CERN Large Hadron Collider (LHC), gluons can play an important role in the dilepton production [78]). For the calculation of the QGP yield in the qualitative analysis of this section, the most simple perturbative QCD cross sections are used for the processes $q + \bar{q} \to l^+l^-$ and $q + \bar{q} \to g + l^+l^-$, assuming $\alpha_S = 0.8$.

Thus we plot the dilepton yields from the reactions $\pi + \pi$ and $q + \bar{q}$, where the pions and quarks have in general different temperatures T_π and $T_{\rm QGP}$. The space-time volumes of the two phases are assumed to be approximately equal. In Fig. 6(a), the gas of pions is assumed to have the temperature $T_\pi = 150$ MeV, while the gas of quarks is assumed to have the temperature $T_{\rm QGP} = 250$ MeV. In Fig. 6(b), we have $T_{\rm QGP} = T_\pi = 190$ MeV.

It has been originally suggested that a window for observing dileptons from the plasma exists in the invariant mass region between the ϕ and J/Ψ peaks [4]. This is supported by the results shown in both Figs. 6(a) and 6(b). However, we see in Fig. 6(a) another region, i.e., $M < 0.5$ GeV, in which the $q + \bar{q}$ annihilation is compatible or even larger than the radiation from the $\pi + \pi$ annihilation; the contribution of the two-to-two process $q + \bar{q} \to g + l^+l^-$ is especially important. The dominance of the thermal yield from quark interactions at masses below $\approx$0.5 GeV is in agreement with the conclusions of Refs. [22,23]. The transport model results of the next section clarify which of the equilibrium scenarios presented in Fig. 6—(a) or (b)—gives a closer resemblance to the channel decomposition of the dilepton production within a microscopic simulation.

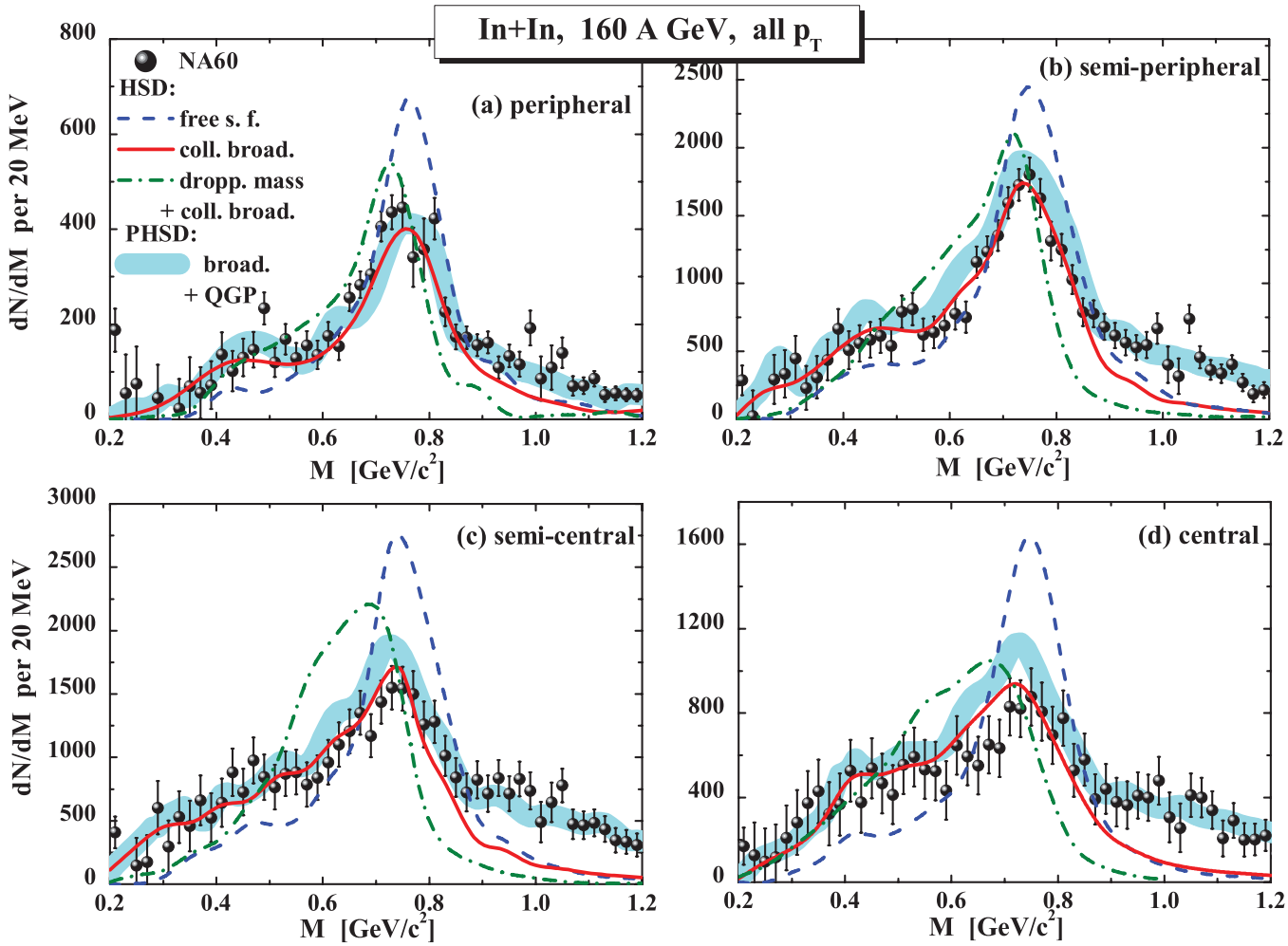

FIG. 7. (Color online) The HSD results for the mass differential dilepton spectra from In + In collisions at 158A GeV in comparison to the excess mass spectrum from the NA60 Collaboration [11]. The actual NA60 acceptance filter and mass resolution have been incorporated [79]. The solid lines show the HSD results for a scenario including the collisional broadening of the ρ meson whereas the dashed lines correspond to calculations with "free" ρ spectral functions for reference. The dash-dotted lines represent the HSD calculations for the dropping mass + collisional broadening model. The wide (light blue) bands represent the PHSD results incorporating direct dilepton radiation from the QGP in addition to a broadened ρ meson.

Of course, the observation of the QGP channels at low mass is possible only after the dilepton yield from the π-, η-, and ω-Dalitz decays is removed. Another word of caution is in place here, because in Fig. 6 the vacuum properties of the ρ meson have been used in plotting the $\pi + \pi$ contribution, whereas the ρ-meson properties are expected to be modified in medium. The modification of the ρ meson will change the size of the new, low-mass window of the QGP observation (cf. next section).

VI. RESULTS AND COMPARISON TO DATA

Let us first note that the bulk properties of heavy-ion reactions at the top SPS energy, such as the number of charged particles, as well as their rapidity, p_T, and transverse energy distributions, were rather well described by PHSD; we refer to Ref. [24] for an extended and detailed comparison to the data. As the lQCD equation of state employed here has a crossover transition, the PHSD calculations show a rather long QGP phase in central In + In collisions at 158A GeV (cf. Fig. 10 of Ref. [24]) with the partonic degrees of freedom dominating for about 3 fm/c. Also, the elementary pp channel is well under control in PHSD as has been demonstrated in Ref. [16].

Previously, by employing the HSD approach to the low-mass dilepton production in relativistic heavy-ion collisions, it was shown in Ref. [16] that the NA60 Collaboration data for the invariant mass spectra of $\mu^+\mu^-$ pairs from In + In collisions at 158A GeV favored the melting ρ scenario [11]. Also the data from the CERES Collaboration [58] showed a preference for the melting ρ picture. For other vector mesons (ω, ϕ), the effects are relatively small, because, due to their much longer lifetimes, ω and ϕ decay predominantly outside the medium after regaining the vacuum properties.

As we see in Fig. 7, the current calculation in the PHSD approach confirms the earlier finding in the hadronic model that the NA60 data favor the scenario of the in-medium

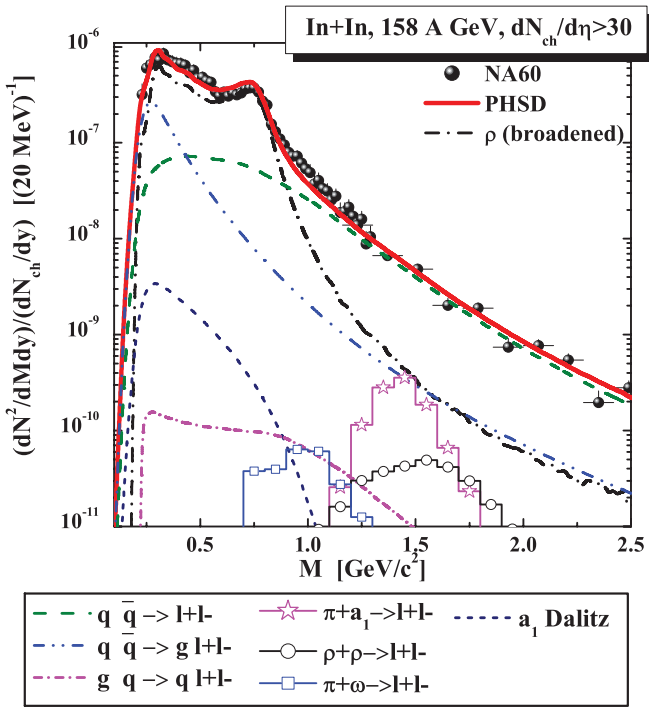

FIG. 8. (Color online) Acceptance-corrected mass spectra of excess dimuons from In + In at 158A GeV integrated over p_T in $0.2 < p_T < 2.4$ GeV from PHSD compared to the data of the NA60 Collaboration [81]. The dash-dotted line shows the dilepton yield from the in-medium ρ with a broadened spectral function, the dashed line presents the yield from the $q + \bar{q}$ annihilation, the dash-dot-dot line gives the contribution of the gluon bremsstrahlung process ($q\bar{q} \to g l^+ l^-$), and the solid line is the sum of all contributions. For the description of the other lines, which correspond to the nondominant channels, please refer to the figure legend.

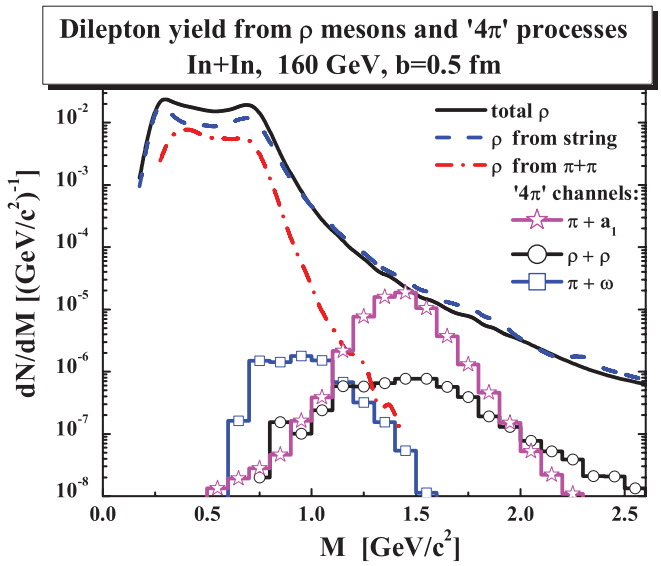

FIG. 9. (Color online) Dilepton radiation from ρ mesons of different origins in PHSD from central In + In collisions at 158A GeV compared to the contributions from the 4π processes ($a_1 + \pi$, $\pi + \omega$, and $\rho + \rho$). The direct ρ mesons produced in mesonic and baryonic strings are given by the dashed line and the thermal ρ mesons produced in $\pi + \pi$ annihilations are given by the dash-dotted line. The contributions of the 4π processes are shown by the lines with symbols: the $\pi + a_1 \to l^+ l^-$ process is displayed by the line with stars, the $\pi + w \to l^+ l^-$ process by the line with squares, and the $\rho + \rho \to l^+ l^-$ process by the line with circles.

broadening of vector mesons. A comparison of the transport calculations to the data of the NA60 Collaborations points toward a melting of the ρ meson at high densities, i.e., a broadening of the vector meson's spectral function in line with the findings of Rapp [80]. No pronounced mass shift of the vector mesons is visible in the data. On the other hand, a closer inspection of Fig. 7 shows that the conventional hadronic sources do not match the measured yield at invariant masses above about 1 GeV/c^2, while the yield at masses close to 1 GeV is reproduced by taking into account the dilepton production channels in the QGP.

The NA60 Collaboration has recently published acceptance-corrected data with the charm contribution subtracted [81]. In Fig. 8 we present PHSD results for the dilepton spectrum excess over the known hadronic sources as produced in In + In reactions at 158A GeV compared to the acceptance-corrected data. We find here that the spectrum at invariant masses in the vicinity of the ρ peak is well reproduced by the ρ meson yield, if a broadening of the meson spectral function in the medium is assumed, while the partonic sources account for the yield at high masses.

One can conclude from Fig. 8 that the measured spectrum for $M > 1$ GeV is dominated by the *partonic* sources. Indeed, the domination of the radiation from the QGP over the hadronic sources in PHSD is related to a rather long—of the order of 3 fm/c—evolution in the partonic phase (in coexistence with the space-time separated hadronic phase) on one hand, cf. Fig. 10 of Ref. [24], and the rather high initial energy densities created in the collision on the other hand, cf. Fig. 6 of Ref. [38].

In addition, we find from Fig. 8 that in PHSD the partonic sources have a considerable contribution to the dilepton yield for $M < 0.6$ GeV. The yield from the two-to-two process $q + \bar{q} \to g + l^+ l^-$ is especially important close to the threshold (≈0.211 GeV). This conclusion from the microscopic calculation is in qualitative agreement with the findings of an early (more schematic) investigation in Ref. [82].

Recalling the illustrative study of dilepton rates in thermal equilibrium in Sec. V, we observe that the nonequilibrium microscopic simulation within the PHSD transport approach qualitatively implies a situation in which the initial partonic phase has temperatures of the order of $T_{\rm QGP} \approx 250$ MeV and the hadron gas in the subsequent evolution has a temperature of $T_\pi \approx 150$ MeV (assuming thermalization and that their evolution is approximately as long). A model scenario in which the temperatures of the partonic and hadronic phases are equal for an extended period of space-time ($T_\pi = T_{\rm QGP} = 190$ MeV) is not supported by the microscopic simulations.

To elucidate the relative importance of the different *hadronic* sources of the excess dileptons in the heavy-ion collisions at top SPS energies, we show in Fig. 9 the channel decomposition of the main hadronic contributions to the dilepton rates in central In + In collisions at 158A GeV integrated over rapidity and p_T. In particular, the dilepton yield

from the decays of the ρ mesons (solid line) is dominantly composed of two channels: the direct ρ mesons produced in mesonic and baryonic strings (dashed line) and the "thermal" ρ mesons produced in $\pi + \pi$ annihilations (dash-dotted line). For comparison, the contributions of the 4π processes are shown by the lines with symbols: the $\pi + a_1 \to l^+l^-$ process is displayed by the line with stars, the $\pi + w \to l^+l^-$ process by the line with squares, and the $\rho + \rho \to l^+l^-$ process by the line with circles. We find that the dilepton yield from the decays of the thermal ρ mesons falls exponentially at high masses. The contributions from the 4π processes start dominating over the yield from the thermal ρ-meson decays at $M \approx 1$ GeV. We further confirm in PHSD that at $M > 1$ GeV the contribution of the $\pi + a_1$ process is the highest among the secondary mesonic sources of the dileptons, as was first noted by the authors of Ref. [64]. On the other hand, in contrast to the thermal ρ mesons, the direct ρ mesons produced in the string decays (following the initial hard collisions) exhibit a power-law tail at masses above 1 GeV and, consequently, dominate the overall dilepton spectrum of hadronic origin for $M > 1$ GeV. Note that the sizable contribution of direct ρ mesons is due to the large hadronic "corona" in In + In collisions at SPS energies.

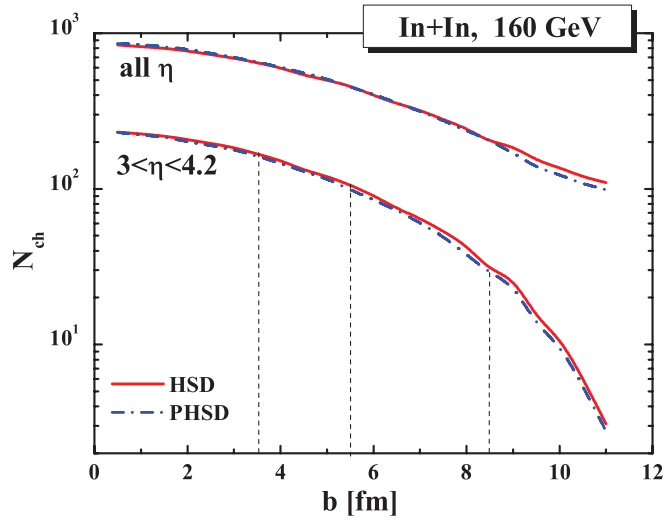

FIG. 11. (Color online) Number of charged particles as a function of the impact parameter from HSD (solid lines) and PHSD (dash-dot lines) integrated over rapidity (upper lines) and within the pseudorapidity acceptance window of the NA60 experiment (lower lines). The vertical dashed lines indicate the different centrality classes.

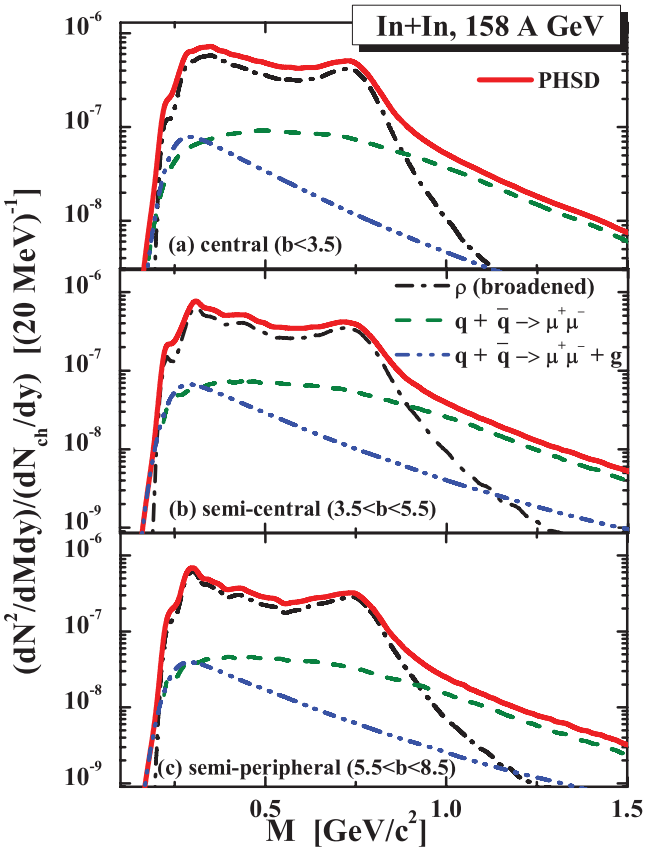

FIG. 10. (Color online) Mass spectra of excess dimuons from In + In at 158A GeV for $0.2 < p_T < 2.4$ GeV and $3 < \eta < 4.2$ from PHSD for different centrality bins. The dash-dotted, dashed, and solid lines show, respectively, the dilepton yield from the in-medium ρ meson with a broadened spectral function, the dilepton yield from the $q + \bar{q}$ annihilation, and the sum of them.

Next we investigate the centrality dependence of the dilepton production in heavy-ion collisions as SPS energies. In Fig. 10 we present the mass spectra of excess dimuons from In + In at 158 AGeV for $0.2 < p_T < 2.4$ GeV and $3 < \eta < 4.2$ from PHSD for different centrality bins. The dash-dotted, dashed, and solid lines show, respectively, the dilepton yield from the in-medium ρ meson with a broadened spectral function, the dilepton yield from the $q + \bar{q}$ annihilation, and the sum of them. We have chosen the following centrality classes: central collisions (impact parameter, 0.5 fm$< b <$ 3.5 fm), semicentral collisions (3.5 fm$< b <$ 5.5 fm), and semiperipheral collisions ($5.5 < b < 8.5$ fm). The predictions in Fig. 10 can be verified/falsified in the future by a direct comparison to the data as the latter become available.

The yields in Fig. 10 are normalized to the number of charged particles N_{ch}. By studying the dependence of N_{ch} on the centrality in In + In collisions at 158A GeV in Fig. 11 we find that PHSD and HSD give very similar results (with only 5% quantitative difference). This finding is in line with the conclusions of the extended study in Ref. [24] that the multiplicities, rapidity distributions, and transverse-momentum distributions of the nonstrange particles produced in heavy-ion collisions at 158A GeV are only weakly sensitive to the presence of a partonic phase with a (crossover) phase transition. The average numbers of charged particles per unit of pseudorapidity in PHSD and HSD for the chosen centrality classes are shown in Table I.

The NA60 Collaboration has accessed the information on the transverse-momentum dependence of dilepton production by measuring the dilepton yield in different bins of p_T. In Fig. 12 we show the mass spectra of excess dimuons from In + In at 158A GeV for different transverse-momentum bins from PHSD compared to the data of the NA60 Collaboration [11,81]. The dash-dot, dash-dot-dot, and solid lines show,

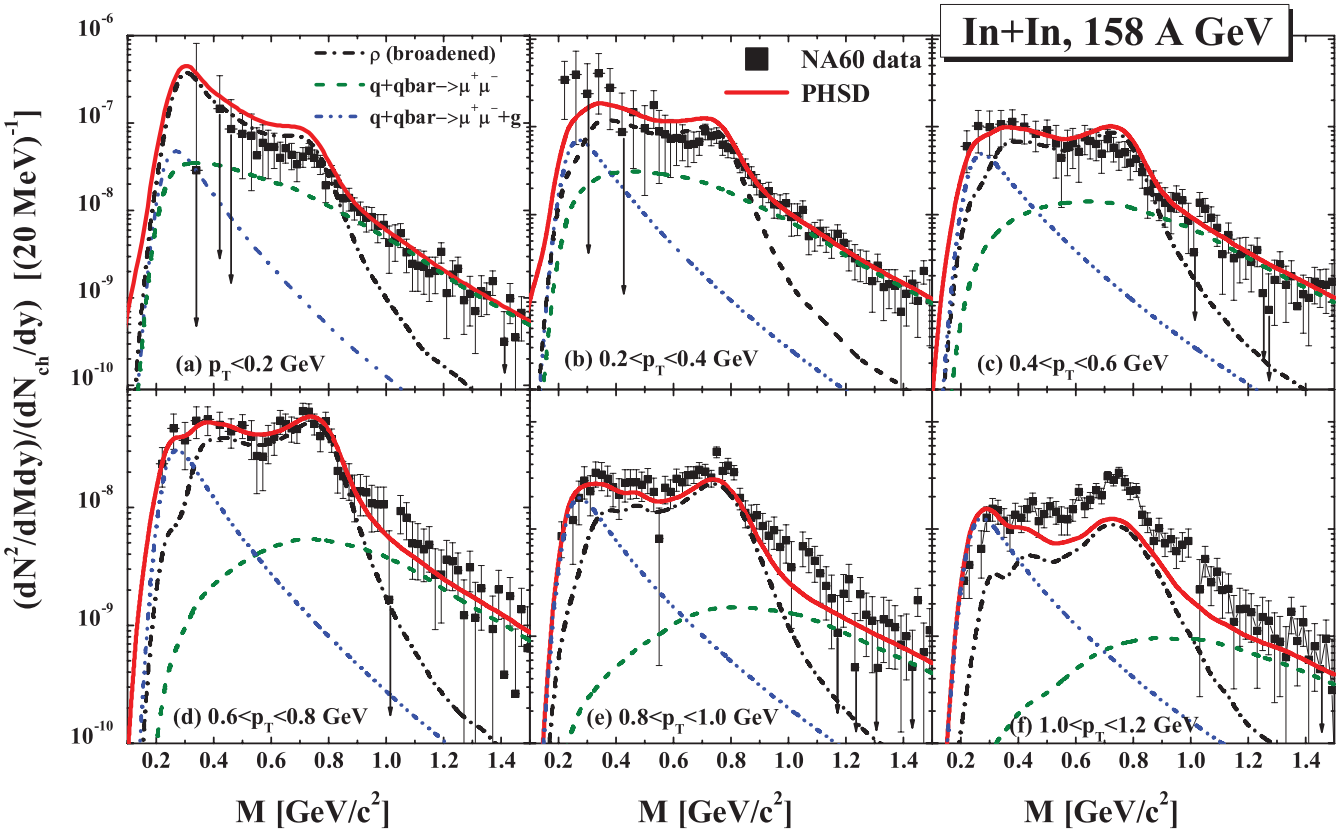

FIG. 12. (Color online) Acceptance-corrected mass spectra of excess dimuons from In + In collisions at 158A GeV for different transverse-momentum bins from PHSD compared to the data of the NA60 Collaboration [11,81]. The dash-dot, dash-dot-dot, and solid lines show, respectively, the dilepton yield from the in-medium ρ meson with a broadened spectral function, the dilepton yield from $q + \bar{q}$, and the sum of them.

respectively, the dilepton yield from the in-medium ρ meson with a broadened spectral function, the dilepton yield from the $q + \bar{q}$ annihilation, and the sum of them. One observes a generally good agreement with the data.

In Fig. 13, transverse mass spectra of dileptons for In + In at 158A GeV in PHSD are compared to the data of the NA60 Collaboration for the four mass bins. The comparison of the mass dependence of the slope parameter evolution in PHSD and the data is shown explicitly in Fig. 14. Including partonic dilepton sources allows us to reproduce in PHSD the m_T spectra (cf. Fig. 13) as well as the finding of the NA60 Collaboration [11,81] that the effective temperature of the dileptons (slope parameters) in the intermediate-mass range is lower than that of the dileptons in the mass bin $0.6 < M < 1$ GeV, which is dominated by hadronic sources (cf. Fig. 14). The softening of the transverse mass spectrum with growing invariant mass

TABLE I. The average numbers of charged particles per unit of pseudorapidity in PHSD and HSD for the different centrality classes.

Centrality	$\langle dN_{\rm ch}/d\eta \rangle$	
	HSD	PHSD
$b < 8.5$ fm	83.44	79.00
$0.5 < b < 3.5$ fm	166.6	157.1
$3.5 < b < 5.5$ fm	119.5	112.6
$5.5 < b < 8.5$ fm	58.13	55.54

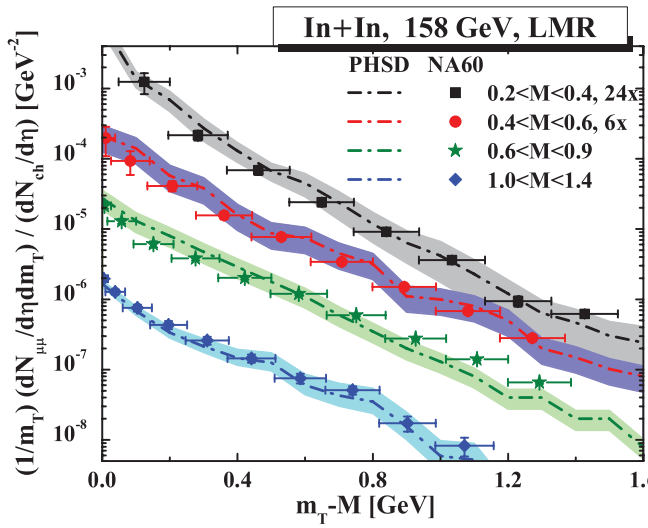

FIG. 13. (Color online) Transverse mass spectra of dileptons for In + In at 158A GeV in PHSD compared to the data of the NA60 Collaboration [11,81].

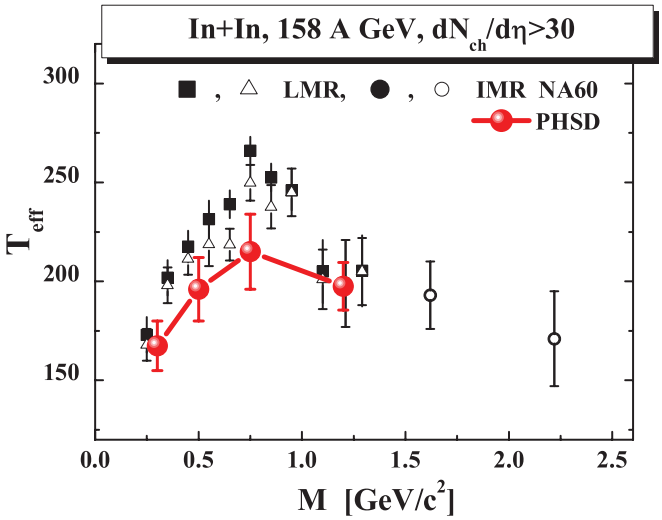

FIG. 14. (Color online) The inverse slope parameter $T_{\rm eff}$ of the dimuon yield from In + In at 158A GeV as a function of the dimuon invariant mass in PHSD compared to the data of the NA60 Collaboration [11,81].

implies that the partonic channels occur dominantly before the collective radial flow has developed. Also, the fact that the slope in the lowest-mass bin and the highest one are approximately equal—both in the data and in PHSD—can be traced back to the two windows of the mass spectrum that in our picture are influenced by the radiation from the sQGP: $M = 2M_\mu - 0.6$ GeV and $M > 1$ GeV (cf. the discussions of Figs. 6 and 8). A detailed look at the PHSD results shows that in total we still slightly underestimate the slope parameter $T_{\rm eff}$ in the ρ-mass region which might be due to missing partonic initial-state effects or to an underestimation of flow in the initial phase of the reaction.

VII. SUMMARY

To address dilepton production in a hot and dense medium as created in heavy-ion collisions, we have employed an up-to-date relativistic transport model, PHSD [24,25]. PHSD consistently describes the full evolution of a relativistic heavy-ion collision from the initial hard scatterings and string formation through the dynamical deconfinement phase transition to the QGP as well as hadronization and to the subsequent interactions in the hadronic phase.

In the present work, we have studied the dilepton production in In + In collisions at 158A GeV within the PHSD off-shell transport approach including a collisional broadening of vector mesons, microscopic secondary multimeson channels, and the strongly interacting QGP radiation, which is described by the interactions of dynamical quasiparticles in line with the degrees of freedom propagated in the transport approach.

A comparison to the data of the NA60 Collaboration shows that the dilepton yield is well described by including the collisional broadening of vector mesons, while simultaneously accounting for the electromagnetic radiation of the sQGP via off-shell quark-antiquark annihilation, quark annihilation with gluon bremsstrahlung, and the gluon-Compton scattering mechanisms.

In particular, the spectra in the intermediate-mass range (1 GeV $\leqslant M \leqslant$ 2.5 GeV) are found to be dominated by quark-antiquark annihilation in the nonperturbative QGP. Also, the observed softening of the transverse mass spectra at intermediate masses (1 GeV $\leqslant M \leqslant$ 2.5 GeV) is approximately reproduced.

Furthermore, for dimuons of low masses ($2M_\mu < M <$ 0.6 GeV), a sizable contribution of partonic processes (in particular, the quark annihilation with the gluon bremsstrahlung) is found, thus possibly providing another window for probing the properties of the sQGP qualitatively in line with the early suggestions in Refs. [8–10].

Our present findings will have to be controlled by dilepton measurements at RHIC and LHC energies, because the PHSD approach is designed to operate also at these higher energies. Our results and predictions for higher energies will be presented in the near future [83].

ACKNOWLEDGMENTS

O.L. and E.L.B. acknowledge financial support through the HIC for FAIR framework of the LOEWE program. V.O. acknowledges financial support from the H-QM and HGS-Hire graduate schools. The work of C.M.K was supported by the US National Science Foundation under Grants No. PHY-0758115 and No. PHY-1068572, the US Department of Energy under Contract No. DE-FG02-10ER41682, and the Welch Foundation under Grant No. A-1358, and he further would like to thank the Frankfurt Institute for Advanced Studies for the warm hospitality during his research visit.

[1] I. Tserruya, in *Relativistic Heavy Ion Physics*, Landolt-Börnstein—Group I Elementary Particles, Nuclei and Atoms, edited by R. Stock (Springer-Verlag, Berlin, Heidelberg, 2010), Vol. 23A.
[2] R. J. Fries, B. Müller, and D. K. Srivastava, Phys. Rev. Lett. **90**, 132301 (2003).
[3] E. V. Shuryak, Sov. Phys. JETP **47**, 212 (1978).
[4] E. V. Shuryak, Phys. Lett. B **78**, 150 (1978); Sov. J. Nucl. Phys. **28**, 408 (1978); Yad. Fiz. **28**, 796 (1978).
[5] E. L. Feinberg, Izv. Akad. Nauk Ser. Fiz. **34**, 1987 (1970).
[6] E. L. Feinberg, Nuovo Cimento A **34**, 391 (1976).
[7] J. D. Bjorken and H. Weisberg, Phys. Rev. D **13**, 1405 (1976).
[8] T. Altherr and P. V. Ruuskanen, Nucl. Phys. B **380**, 377 (1992).
[9] K. Haglin, C. Gale, and V. Emel'yanov, Phys. Rev. D **47**, 973 (1993).
[10] D. Pal, K. Haglin, and D. Srivastava, Phys. Rev. C **54**, 1366 (1996).
[11] R. Arnaldi *et al.* (NA60 Collaboration), Phys. Rev. Lett. **96**, 162302 (2006); J. Seixas *et al.*, J. Phys. G **34**, S1023 (2007); S. Damjanovic *et al.*, Nucl. Phys. A **783**, 327c (2007); R. Arnaldi *et al.*, Eur. Phys. J. C **61**, 711 (2009).

[12] R. Rapp, J. Wambach, and H. van Hees, in *Relativistic Heavy-Ion Physics*, edited by R. Stock (Landolt-Boernstein, 2010), Vol. 1-23A.
[13] O. Linnyk, E. L. Bratkovskaya, and W. Cassing, Nucl. Phys. A **830**, 491c (2009).
[14] O. Linnyk, W. Cassing, E. L. Bratkovskaya, and J. Manninen, Nucl. Phys. A **855**, 273 (2011).
[15] W. Cassing and E. L. Bratkovskaya, Phys. Rep. **308**, 65 (1999).
[16] E. L. Bratkovskaya, W. Cassing, and O. Linnyk, Phys. Lett. B **670**, 428 (2009).
[17] K. Dusling, D. Teaney, and I. Zahed, Phys. Rev. C **75**, 024908 (2007); K. Dusling and I. Zahed, *ibid.* **80**, 014902 (2009); Nucl. Phys. A **825**, 212 (2009).
[18] T. Renk and J. Ruppert, Phys. Rev. C **77**, 024907 (2008); J. Ruppert, C. Gale, T. Renk, P. Lichard, and J. I. Kapusta, Phys. Rev. Lett. **100**, 162301 (2008).
[19] H. van Hees and R. Rapp, Phys. Rev. Lett. **97**, 102301 (2006).
[20] H. van Hees and R. Rapp, Nucl. Phys. A **806**, 339 (2008).
[21] T. Song, K. C. Han, and C. M. Ko, Phys. Rev. C **83**, 024904 (2011).
[22] K. Gallmeister, B. Kämpfer, and O. P. Pavlenko, Phys. Lett. B **473**, 20 (2000).
[23] K. Gallmeister, B. Kämpfer, O. P. Pavlenko, and C. Gale, Nucl. Phys. A **688**, 939 (2001).
[24] W. Cassing and E. L. Bratkovskaya, Nucl. Phys. A **831**, 215 (2009).
[25] E. L. Bratkovskaya, W. Cassing, V. P. Konchakovski, and O. Linnyk, Nucl. Phys. A **856**, 162 (2011).
[26] E. L. Bratkovskaya and W. Cassing, Nucl. Phys. A **619**, 413 (1997).
[27] W. Ehehalt and W. Cassing, Nucl. Phys. A **602**, 449 (1996).
[28] W. Cassing and S. Juchem, Nucl. Phys. A **665**, 377 (2000); **672**, 417 (2000).
[29] E. L. Bratkovskaya and W. Cassing, Nucl. Phys. A **807**, 214 (2008).
[30] W. Cassing, Eur. Phys. J. (Special Topics) **168**, 3 (2009).
[31] A. Peshier, Phys. Rev. D **70**, 034016 (2004); J. Phys. G **31**, S371 (2005).
[32] A. Peshier and W. Cassing, Phys. Rev. Lett. **94**, 172301 (2005).
[33] A. Peshier, B. Kämpfer, O. P. Pavlenko, and G. Soff, Phys. Rev. D **54**, 2399 (1996); P. Levai and U. Heinz, Phys. Rev. C **57**, 1879 (1998); A. Peshier, B. Kämpfer, and G. Soff, *ibid.* **61**, 045203 (2000); Phys. Rev. D **66**, 094003 (2002); M. Bluhm, B. Kampfer, R. Schulze, D. Seipt, and U. Heinz, Phys. Rev. C **76**, 034901 (2007).
[34] W. Cassing and E. L. Bratkovskaya, Phys. Rev. C **78**, 034919 (2008).
[35] O. Linnyk, E. L. Bratkovskaya, J. Manninen, and W. Cassing, J. Phys. Conf. Ser. **312**, 012010 (2011).
[36] O. Linnyk, J. Phys. G **38**, 025105 (2011); O. Linnyk, S. Leupold, U. Mosel, Phys. Rev. D **71**, 034009 (2005); **75**, 059901(E) (2007).
[37] J. Manninen, E. L. Bratkovskaya, W. Cassing, and O. Linnyk, Eur. Phys. J. C **71**, 1615 (2011).
[38] O. Linnyk, E. L. Bratkovskaya, and W. Cassing, Int. J. Mod. Phys. E **17**, 1367 (2008); O. Linnyk, E. L. Bratkovskaya, W. Cassing, and H. Stöcker, Phys. Rev. C **76**, 041901 (2007).
[39] G. E. Brown and M. Rho, Phys. Rev. Lett. **66**, 2720 (1991); Phys. Rep. **363**, 85 (2002).
[40] T. Hatsuda and S. H. Lee, Phys. Rev. C **46**, R34 (1992).
[41] M. Asakawa and C.-M. Ko, Phys. Rev. C **48**, R526 (1993).
[42] C. M. Shakin and W.-D. Sun, Phys. Rev. C **49**, 1185 (1994).
[43] F. Klingl and W. Weise, Nucl. Phys. A **606**, 329 (1996); F. Klingl, N. Kaiser, and W. Weise, *ibid.* **624**, 527 (1997).
[44] S. Leupold, W. Peters, and U. Mosel, Nucl. Phys. A **628**, 311 (1998).
[45] G. Chanfray, R. Rapp, and J. Wambach, Phys. Rev. Lett. **76**, 368 (1996); R. Rapp, G. Chanfray, and J. Wambach, Nucl. Phys. A **617**, 472 (1997).
[46] W. Peters, M. Post, H. Lenske, S. Leupold, and U. Mosel, Nucl. Phys. A **632**, 109 (1998); M. Post, S. Leupold, and U. Mosel, *ibid.* **689**, 753 (2001).
[47] R. Rapp and J. Wambach, Adv. Nucl. Phys. **25**, 1 (2000).
[48] C. Song, S. H. Lee, and C. M. Ko, Phys. Rev. C **52**, 476 (1995).
[49] C. Song, V. Koch, S. H. Lee, and C. M. Ko, Phys. Lett. B **366**, 379 (1996).
[50] G. Agakichiev *et al.* (CERES Collaboration), Phys. Rev. Lett. **75**, 1272 (1995); Th. Ullrich *et al.*, Nucl. Phys. A **610**, 317c (1996); A. Drees, *ibid.* **610**, 536c (1996).
[51] M. A. Mazzoni (HELIOS Collaboration), Nucl. Phys. A **566**, 95c (1994); M. Masera, *ibid.* **590**, 93c (1995); T. Åkesson *et al.*, Z. Phys. C **68**, 47 (1995).
[52] G. Q. Li, C. M. Ko, and G. E. Brown, Phys. Rev. Lett. **75**, 4007 (1995).
[53] C. M. Ko, G. Q. Li, G. E. Brown, and H. Sorge, Nucl. Phys. A **610**, 342c (1996).
[54] W. Cassing, W. Ehehalt, and C. M. Ko, Phys. Lett. B **363**, 35 (1995).
[55] C. Ernst, S. A. Bass, M. Belkacem, H. Stocker, and W. Greiner, Phys. Rev. C **58**, 447 (1998).
[56] W. Cassing, E. L. Bratkovskaya, R. Rapp, and J. Wambach, Phys. Rev. C **57**, 916 (1998).
[57] I. Tserruya, Nucl. Phys. A **681**, 133c (2001); Eur. Phys. J. **43C**, 399 (2005).
[58] D. Adamova *et al.* (CERES Collaboration), Nucl. Phys. A **715**, 262 (2003); (CERES Collaboration), Phys. Rev. Lett. **91**, 042301 (2003); G. Agakichiev *et al.*, Eur. Phys. J. C **41**, 475 (2005) ; D. Adamova *et al.* Phys. Lett. B **666**, 425 (2008).
[59] J. Ruppert, T. Renk, and B. Müller, Phys. Rev. C **73**, 034907 (2006).
[60] E. L. Bratkovskaya and C. M. Ko, Phys. Lett. B **445**, 265 (1999).
[61] W. Cassing, Y. S. Golubeva, A. S. Iljinov, and L. A. Kondratyuk, Phys. Lett. B **396**, 26 (1997); Y. S. Golubeva, L. A. Kondratyuk, and W. Cassing, Nucl. Phys. A **625**, 832 (1997).
[62] V. Metag, Prog. Part. Nucl. Phys. **61**, 245 (2008).
[63] E. Santini, J. Steinheimer, M. Bleicher, and S. Schramm, Phys. Rev. C **84**, 014901 (2011).
[64] C. Song, C. M. Ko, and C. Gale, Phys. Rev. D **50**, 1827 (1994).
[65] C. Gale and P. Lichard, Phys. Rev. D **49**, 3338 (1994).
[66] G.-Q. Li and C. Gale, Phys. Rev. C **58**, 2914 (1998).
[67] C. Gale and J. Kapusta, Phys. Rev. C **35**, 2107 (1987); **38**, 2659 (1988).
[68] K. Haglin and C. Gale, Phys. Rev. D **52**, 6297 (1995).
[69] V. Aulchenko *et al.*, Novosibirsk Report No. 86-106, 1986.
[70] R. Baldini-Ferroli, in *Hadronic Physics at Intermediate Energy: 2nd: Winter School Proceedings*, edited by T. Bressani, B. Menetti, and G. Pauli, (Elsevier, Amsterdam/New York, 1987).

[71] A. Antonelli *et al.* (DM2 Collaboration), Z. Phys. C **56**, 15 (1992).
[72] S. Dolinsky *et al.* (ND Collaboration), Phys. Rep. **202**, 99 (1991).
[73] N. Albrecht *et al.* (ARGUS Collaboration), Phys. Lett. B **185**, 223 (1987).
[74] C. Bacci *et al.* ($\gamma\gamma 2$ Collaboration), Nucl. Phys. B **184**, 31 (1981).
[75] A. Cordier *et al.* (M3N Collaboration), Phys. Lett. B **109**, 129 (1982).
[76] C. Song and C. M. Ko, Phys. Rev. C **53**, 2371 (1996).
[77] E. L. Bratkovskaya, S. M. Kiselev, and G. B. Sharkov, Phys. Rev. C **78**, 034905 (2008).
[78] Z.-W. Lin and C. M. Ko, Nucl. Phys. A **671**, 567 (2000).
[79] S. Damjanovic (private communication).
[80] R. Rapp (private communication); arXiv:nucl-th/0204003.
[81] R. Arnaldi *et al.* (NA60 Collaboration), Eur. Phys. J. C **59**, 607 (2009).
[82] J. Alam, T. Hirano, J. K. Nayak, and B. Sinha, arXiv:0902.0446.
[83] O. Linnyk *et al.*, arXiv:1111.2975 [nucl-th].